Reduced fast electron transport in shock-heated plasma in multilayer targets due to self-generated magnetic fields

C. McGuffey,[1] J. May,[2] T. Yabuuchi,[1] H. Sawada,[1] M. S. Wei,[3] R. B. Stephens,[3] C. Stoeckl,[4] W. B. Mori,[2] H. S. McLean,[5] P. K. Patel,[5] and F. N. Beg[1]

[1]*Center for Energy Research, University of California, San Diego, La Jolla, California 92093-0417, USA*
[2]*Department of Physics and Astronomy, University of California, Los Angeles, Los Angeles, California 90095, USA*
[3]*General Atomics, P.O. Box 85608, San Diego, California 92186-5608, USA*
[4]*Laboratory for Laser Energetics, University of Rochester, Rochester, New York 14623, USA*
[5]*Lawrence Livermore National Laboratory, Livermore, California 94550, USA*

(Received 14 April 2018; published 17 September 2018)

Fast electron transport has been studied in cold solid density CH, cold CH foam (200 mg/cm^3), and CH plasma (40 eV 30 mg/cm^3) targets—the latter created by shocking the CH foam with a 1.2 kJ long pulse laser and allowing it to expand. The fast electrons were produced using the OMEGA EP laser pulse (800 J, 8 ps) incident on a Au flat target. With the CH plasma, the fluence of fast electrons reaching a Cu foil at the far side of the transport was reduced significantly (25× weaker peak $K\alpha$ emission). Particle-in-cell simulations using the OSIRIS code modeled fast electron transport in the unshocked foam and plasma cases assuming fixed ionization and including source generation, transport in Au and CH layers, Coulomb collisions, and refluxing. Simulations indicate two main mechanisms which alter electron energy transport through the target between the foam and plasma cases, both due to the magnetic field: a collimating field in the CH region, caused by the resistivity of the return current and more prevalent in the foam; and an insulating field at the Au-CH interface, present only with the plasma.

DOI: 10.1103/PhysRevE.98.033208

I. INTRODUCTION

The interaction of a short pulse, relativistic intensity laser with above critical-density plasma results in efficient energy transfer into a beam of fast electrons. The source parameters and transport characteristics in cold material and warm plasma have important implications for uses such as fast ignition (FI) fusion [1], in which > MeV charged particles (typically electrons) must deposit sufficient energy into dense fuel [2]. Transport of the high current beams required can be impacted by filamentation [3], anomalous stopping [4], and other complexities as summarized in Ref. [5]. Transport of fast electrons has been studied computationally using hybrid particle-in-cell (PIC) codes [6,7], and experimentally in planar geometry [8,9], allowing measurement of the electron beam transverse profile at slices along its trajectory. However, the transport layers in those experimental studies were initially cold solid material. Pérez *et al.* [10] conducted an experiment to investigate fast electron transport through cylindrically imploded plasma. It was noted that electron beam transport fell off rapidly as the material underwent implosion, but in their follow-up studies [11], x-ray and proton radiography were compared to hydrodynamic simulations, which determined that large temperature and density gradients could have existed in the radial dimension. Reference [12] showed that those gradients could have created magnetic fields capable of affecting the transport. A more recent study [13] used a short pulse and counterpropagating long pulse to avoid such complications. The resistive and collisional stopping powers were measured using a 35 J, 1.5 ps short pulse driver. It was estimated that with a higher energy, multipicosecond driver, the two powers would be comparable, and for even higher currents relevant to FI, resistive stopping would remain low.

II. EXPERIMENTAL CONFIGURATION

In this article, we present experimental and PIC simulations of short pulse, high intensity laser-generated fast electron transport, with significantly longer pulse length and higher total energy (8 ps and 800 J). It is a systematic comparative study of transport of a FI-relevant electron source through both an initially cold plastic (CH) and a large volume uniform plasma state. We show differences between transport in cold material and uniform warm plasma: copper (Cu) $K\alpha$ (produced when fast electrons collide with atoms of a Cu foil at the end of the transport medium) was reduced by a factor of 25 with the plasma compared to the foam. PIC modeling indicates that the cause of the difference is shared by two effects: a resistive collimating magnetic field throughout the denser and (initially) cold foam, and an insulating magnetic field at the interface between the gold (Au) electron source layer and the lower density CH plasma.

Experiments were conducted at the OMEGA EP facility [14]. Targets consisted of a Au foil for fast electron generation, a CH transport layer, and a Cu observation foil. The CH layer was either a solid CH foil (50 μm-thick, 1 g/cm^3, $\rho r = 5$ mg/cm^2) or a CH foam (250 μm-thick, 200 mg/cm^3,

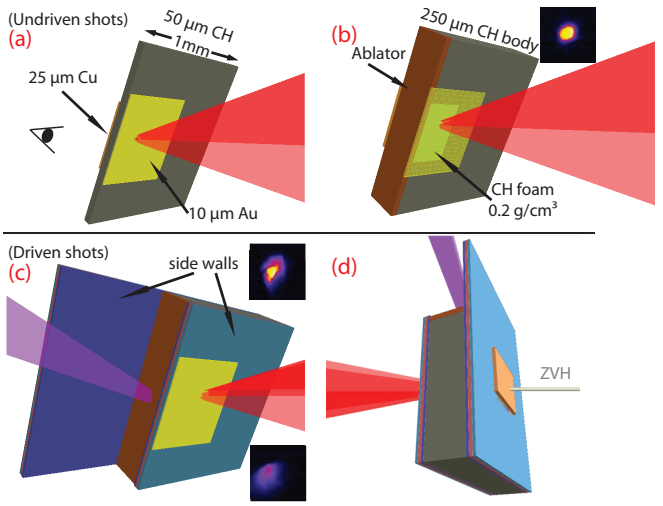

FIG. 1. Fast electrons from short pulse laser (red) interaction with a Au foil transported through three different CH layers: solid foil (a), foam (b), and foam heated to plasma by a 1.2 kJ beam [purple in (c) and (d)]. The Au foil is shown partially transparent in (b) to reveal the foam. A Cu foil was behind the transport layers. (d) The perspective of the Spherical Crystal Imager and also indicating the line of sight of the Zn Von Hamos spectrometer. Pinhole camera images of the interaction are shown in the inset.

$\rho r = 5$ mg/cm^2), and the foam was either in its original form, or else was driven from the side to produce a longitudinally uniform, expanded plasma. To be confident that a large, uniform, well-defined plasma was created, a platform for characterizing the plasma transport volume was first developed with OMEGA EP as reported in [15,16]. The plasma was created by shock heating a CH foam (250 μm thick and 250 μm by 400 μm in the transverse dimensions) using a ~1.2 kJ 3.5 ns UV laser driver pulse incident on a side ablator wall, and was characterized using x-ray absorption spectroscopy. The plasma was determined to be in a relatively steady-state condition 7 ns after incidence of the laser driver, having density 30 ± 10 mg/cm^3 and temperature 40 ± 5 eV at the position probed. The same target and laser drive were used for the driven foam shots in this experiment, with the UV pulse incident 4 or 7 ns before the short pulse. A side wall prevented the interactions from interfering with the measurement and also gave room for the plasma to expand (full volume 360 μm thick and 250 μm by 400 μm transversely). The three target types are shown in Fig. 1.

The short pulse delivered 266 J (infrared) in 8.5 ps for the solid CH target shot and 764 ± 10 J in 8.1 ± 0.1 ps for all other shots, at 25° incidence angle, corresponding to a normalized vector potential of 3. The driver pulse delivered 1231 ± 49 J (ultraviolet) in 3.5 ns onto the ablator surface.

The emission from the Cu foil was diagnosed both spatially using a spherical crystal imager (SCI) [17] and spectrally using a von Hamos highly oriented pyrolytic graphite (HOPG) spectrometer (ZVH), which has a ~2 keV spectral window and was tuned to measure Cu *K*-shell emission. These emission diagnostics used imaging plates, which use photostimulated luminescence (PSL) as the unit of measurement.

III. RESULTS: MAJOR REDUCTION IN COPPER EMISSION FOR THE DRIVEN PLASMA TRANSPORT LAYER

For the solid CH target, the Cu $K\alpha$ emission profile was localized in the center of the foil indicating a directional electron beam with transport somewhat controlled by resistive collimation, typical of similar experiments in the literature [18,19]. The shape of the Cu $K\alpha$ emission from the unshocked foam target was similar to the solid CH case with comparable peak brightness and integrated signal after taking into account the longer foil separation and higher laser power. However, the observed signals from both Cu $K\alpha$ diagnostics indicate a much stronger difference between the (undriven) foam and (driven) plasma transport layer cases as seen in the raw images, lineouts, and signal levels shown in Fig. 2. The emission from all driven shots was dispersed over the foil with no apparent features, and the emission was significantly dimmer. The SCI signal from a driver-only shot was subtracted from the driven shots; the remaining signal was reduced compared to the undriven shots by a factor of 16.3 ± 1.8 when comparing the spatially integrated SCI signal and 18.1 ± 1.3 when

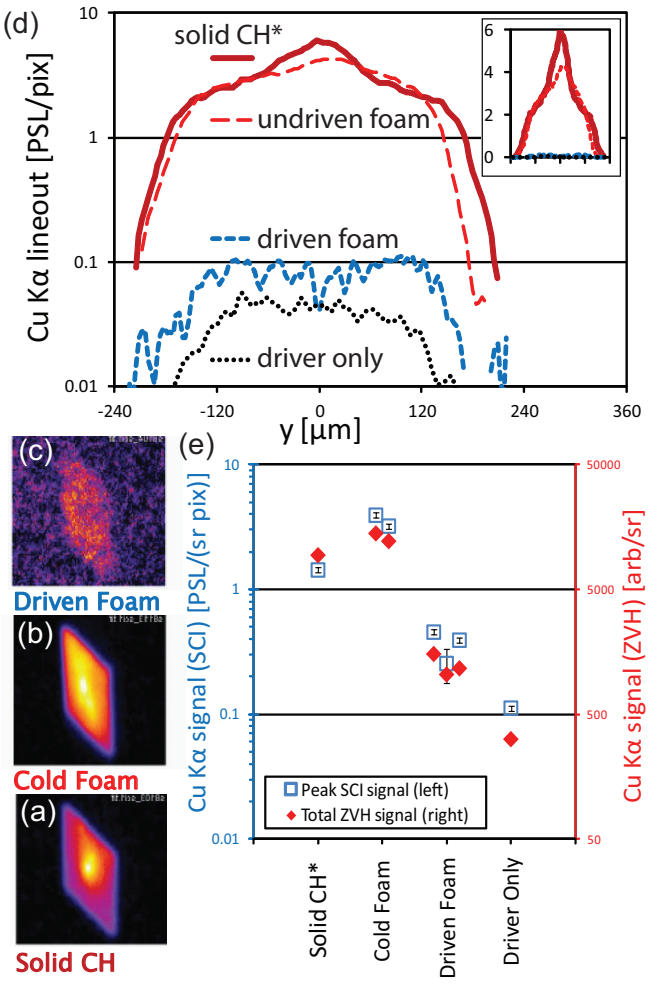

FIG. 2. Spherical Crystal Imager images of the Cu $K\alpha$ emission [(a)–(c), each normalized individually]. Filter-corrected lineouts are plotted (d) and the signals from the SCI and ZVH are analyzed (e). *The solid CH data have been scaled by laser power.

comparing the area under the Cu $K\alpha$ peaks on the separate ZVH diagnostic. The corresponding ratio for the peak angular intensity as measured with the SCI was 25.0 ± 2.5.

The short pulse laser-plasma interaction was monitored on each shot using x-ray pinhole camera (XRPHC) images of the interaction. Of the three driven shots, two showed evidence of disruption [XRPHC shown in Fig. 1(c), lower inset] while the third showed minor disruption [Fig. 1(c), upper inset]—the XRPHC intensity was only diminished by 7% as compared to the undriven shots.

IV. SIMULATIONS SHOW UNCOLLIMATED TRANSPORT AND INTERFACE EFFECTS FOR THE LOW DENSITY PLASMA

Two-dimensional (2D) PIC simulations were conducted using the OSIRIS code [20] to examine the particles' behavior in the target and explain the differences observed in transport between the foam and plasma cases. The cold, solid case is not modeled. The simulations presented had the following parameters. The plasma region was 300 μm wide and uniform transversely; 260 μm in the longitudinal direction, consisting of a 10 μm Au layer in front of a 250 μm CH layer. The plasma was separated on all sides from the simulation edge by 10 μm of vacuum. The Au region had a charge density of 392 n_c—where n_c is the critical density for a 1 μm wavelength laser—a charge state of $Z = 8$ (pertinent only for Coulomb collisions) and a mass-to-charge ratio of $4.5 \times 10^4\, m_e/e$. The CH layer had a mass-to-charge ratio of 3600 m_e/e, a charge density of either 7 n_c (consistent with the lower end of the inferred plasma density, ~22 mg/cm^3, referred to as the "plasma" case from now on) or 63 n_c (consistent with the cold foam density, referred to as "foam" from now on), and a charge state of $Z = 6$ (separate C and H ions were not modeled). In the plasma case, the electrons and ions in the CH layer were initialized with a temperature of 40 eV, and the Au layer was in pressure balance; in the foam case the entire target was initialized at room temperature. A laser was focused on the center of the Au region, with a wavelength of $\lambda = 1$ μm, a spot size (FWHM) of 34 μm, and a normalized vector potential of $a_0 = Ae/m_e c = 3$. Incidence was normal to the surface and the electric field was in the plane of the simulation; the laser rise time was one laser period, after which the intensity remained constant.

The OMEGA EP laser system has a prepulse phase with duration of order nanosecond, and omitting this phase (which cannot be modeled practically in OSIRIS) results in a sharper initial vacuum-matter interface and consequently a somewhat cooler fast electron population [21]. The accelerated electron beam will be otherwise broadly similar, and more importantly, this approach uses the same idealized laser pulse in the foam and plasma simulations, so the differences between the two will map to the differences between the corresponding experimental cases, even if the exact beam profile has differences between simulation and experiment.

The numerical parameters were as follows. The cell size was 0.075 c/ω_0 square, and the time step was $0.05/\omega_0$. In the Au layer there were 224 electrons and ions per cell, in the CH layer the number was either 36 or 4 for the foam or plasma case, respectively. Boundary conditions were periodic transversely; longitudinally they were absorbing (perfectly matched layer) for fields and reflecting for particles. Particle splitting was used for the high-energy particles, with up to six splits, to reduce macroparticle stopping [22]. Coulomb collisions were included using the model of Pérez *et al.* [23] including the low-temperature correction explained therein.

The top row of Fig. 3 shows the forward heat flux (energy transport) from these simulations at time $t = 6.3$ ps; the results from the foam and plasma cases are in the left and right columns, respectively. We focus on the heat transport, the third moment of the distribution function, as it is the lowest moment closely associated with the transport of the fast electrons. The first moment—the net electron current—will be near zero because the current of the fast electrons is almost exactly canceled by a cold return current, necessary to prevent change buildup at the surface. There is no such cancellation of energy transport, and as the temperature of the background return current is much lower than the kinetic energy of the fast electron beam, the background electrons will contribute negligibly to the heat flux which will therefore be dominated by the fast electrons. In the foam, the heat flux can be seen emerging from the laser interaction region as a number of filaments. The outermost filaments continue into the foam along straight paths, at roughly 45° above and below the middle of the box; the more interior filaments, however, remain near the middle of the box or curve back towards it as they cross the foam, with one filament each above and below the main heat flux region clearly bending back in and merging into other filaments. The net effect is that the majority of the heat transport coalesced into a single, albeit filamented, beam along the direction of target normal.

The heat flux in the plasma case also shows a filamented structure, but the individual filaments fan out in straight paths without collimating or in any other way interacting. In addition, the filaments, with the exception of one in the middle of the box, are notably weaker than those in the foam case. Heat can also be seen entering the plasma above and below the laser interaction region.

The bottom row of Fig. 3 shows the magnetic field at the same time. In both the foam and the plasma cases the same filamentary structure present in the heat flux can be seen in the B field, with collimating fields (for forward going electrons) wrapping around each energy beam. In the foam case a weaker, global collimating field is also present around the bundle of filaments, causing them to converge.

In the plasma case the field near the Au-CH interface is shown as an insert with a different color scale to show a wider range of field strength. In this region a large, strong, turbulent field can be seen, with transverse width somewhat greater than the laser spot size, and magnitude of over 100 MG (equivalent to greater than unity in simulation units of $m_e c\, \omega_0/e$). Close to the middle of the box this field switches sign—and hence goes through zero—and it can be seen that it is from this field null that the one strong heat flux filament emerges. There is no similar interface field in the foam case.

To emulate the Cu layer in the experiment, the total energy density in the electrons in a 20 μm-thick region at the far side of the target was integrated. Figure 4 shows this value, time averaged over the duration of the simulation (6.3 ps) and smoothed by 20 μm to approximate the effective optical

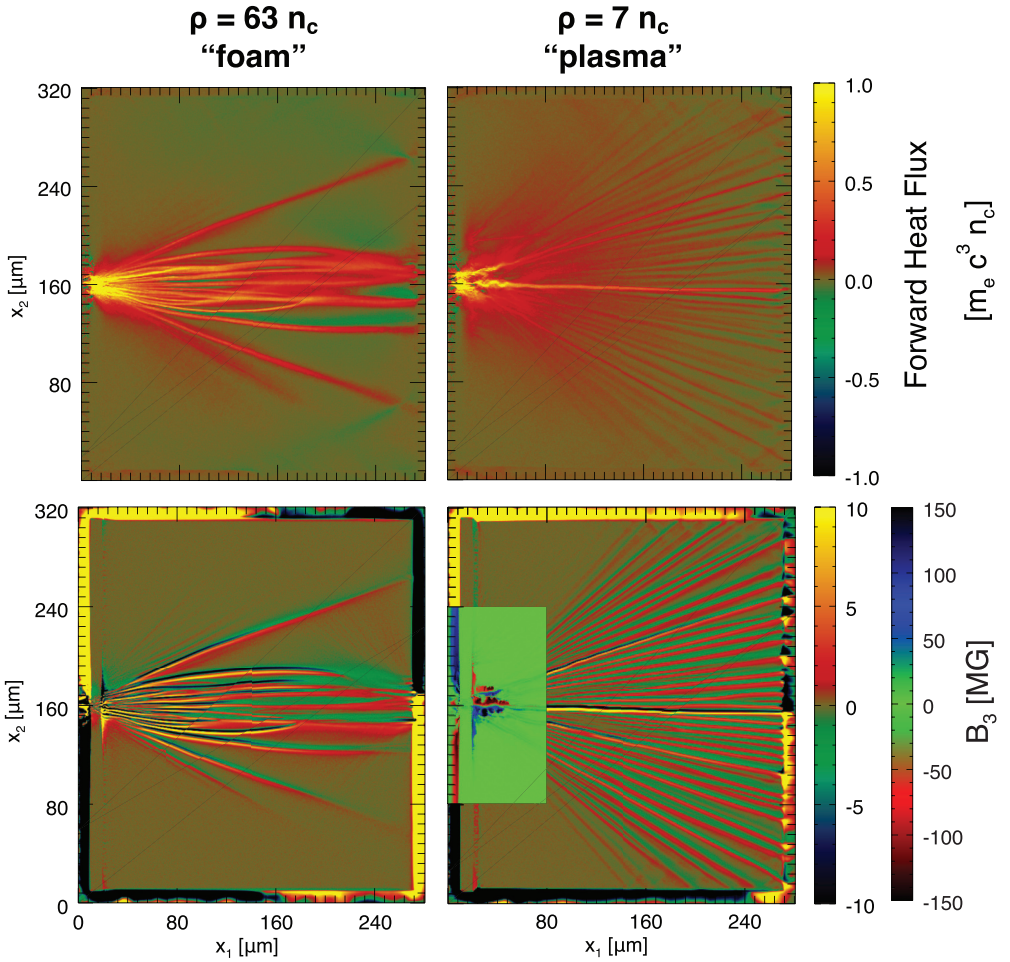

FIG. 3. (Left column) Higher density "foam" case; (right column) lower density "plasma" case. (Top row) Forward heat flux at $t = 6.3$ ps. (Bottom row) Magnetic field at $t = 6.3$ ps. In the plasma case the strong field at the Au/CH interface is shown with enhanced color scale.

resolution of the SCI. Both the foam and plasma cases show a baseline energy density of about 0.1 $m_e c^2 n_c$, which is likely an overestimate compared to reality due to the 2D geometry and finite target in the simulation creating a smaller region for the refluxing electrons to deposit their energy. In the foam simulation, a narrow peak can be seen well above the baseline in the same region where the main heat flux beam is directed; two smaller peaks can also just be made out at the same location as the two filaments which are not trapped in the main beam. Contrasting this the signal from the plasma case shows almost no features above baseline. This is consistent with the experimental $K\alpha$ signal, although the peak is narrower in the simulation results.

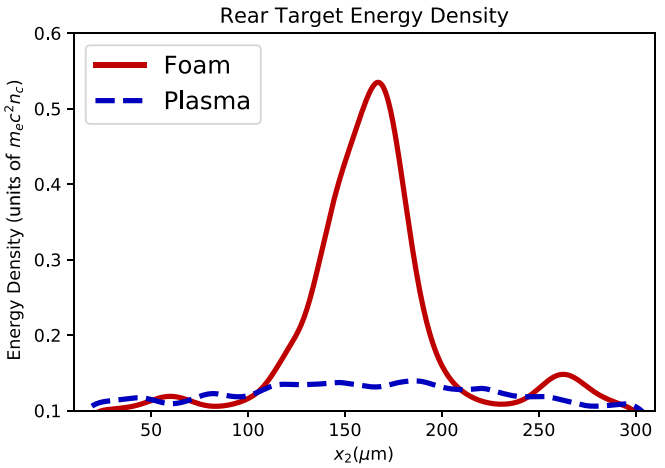

FIG. 4. Total energy density in the electrons in the rear 20 μm of the simulation target averaged over 6.3 ps, for both plasma and foam cases.

V. DISCUSSION

It appears from these diagnostics that the flow of high-energy electrons which are accelerated by the laser is determined by the structure of the magnetic field. The growth of that field can in part be determined by expressing the electric field using a generalized Ohm's law [24] which retains the resistivity and $\mathbf{V} \times \mathbf{B}$ terms, and then inserting that into Faraday's law:

$$\partial \mathbf{B}/\partial t = -c\nabla \times \mathbf{E} = \nabla \times (c\,\eta\,\mathbf{j}_{\text{fast}} + (\mathbf{V} \times \mathbf{B})), \quad (1)$$

where $\mathbf{j}_{\text{fast}}$ is the current of the high energy electrons, η is the effective resistivity due to the collisionality of the return

current, $\mathbf{V}$ is the material flow of the plasma defined as $\mathbf{V} \equiv \frac{\sum_{s=e,i} v_s m_s n_s}{\sum_{s=e,i} m_s n_s}$, and we have assumed that $\mathbf{j}_{\text{fast}} = -\mathbf{j}_{\text{return}}$, that is that the net current is near zero.

If the resistivity is assumed to be constant in space, the first term will lead to the growth of a collimating magnetic field [25]; it can also lead to breakup of the beam into multiple filaments [26]. In the foam case both effects are seen, with the beam breaking up into filaments quickly upon entering the CH region but then mostly collimating before crossing the box; in the plasma simulation only filamentation can be seen, with no indication of collimation.

The distinction between the plasma and foam cases which leads the difference in behavior appears to be the initial density; the reason is that the effect of ohmic heating due to the return current is to cause a gradient in the resistivity which opposes the collimation, and the lower density CH is able to heat more rapidly. Although the initial temperature may also have some effect on the collisionality, both targets quickly heat up from the short-pulse interaction such that the initial temperature is irrelevent; simulations of reduced-size target show no initial temperature effect on the heat flux behavior (though such targets do warm more rapidly due to their lower total simulated mass).

The second term on the right-hand side of the Ohm's law describes the trapped flow of the magnetic field with material current, which can be seen by dropping the resistive term from the equation and using the continuity equation, $\frac{\partial \rho}{\partial t} + \nabla \cdot (\mathbf{V}\rho) = 0$, and the definition of the convective derivative $\frac{D}{Dt} = \frac{\partial}{\partial t} + \mathbf{V} \cdot \nabla$, to arrive at

$$\frac{D}{Dt}\left(\frac{\mathbf{B}}{\rho}\right) = \frac{1}{\rho}(\mathbf{B} \cdot \nabla)\mathbf{V}. \tag{2}$$

This equation shows that the ratio of the magnetic field strength to the material density is a convective constant except where the material current varies in the direction of the field. In two-dimensional situations such as the simulations presented here the analysis is even simpler, as the self-generated magnetic field can only point out of the plane and so the right-hand side is exactly zero; in this case the ratio of field strength to density is an explicit convective constant (again, when the other terms in the Ohm's law are neglected). This term causes magnetic field which is created in the plastic region to be carried with the return current back toward the laser. This appears to be the origin of the strong, turbulent field region at the Au-CH interface in the plasma case, which can be seen growing continuously in time as the field flows back toward the focus. With strength above unity in simulation units, the Larmor radius in this field of even a particle at twice the laser quiver velocity [27] is less than a micron, significantly smaller than the spatial extent of the field region. This field inhibits the ability of electrons to enter the CH region, causing electrons to exit the gold away from the laser focus and trapping more heat in the gold; it also affects the formation and evolution of the heat flux filaments, for instance, preventing strong filaments from entering the plasma except where they can pass through the field region along field nulls. In the foam the growth rate of this interface field is significantly lower as the velocity of the plasma making up the return current is less, such that no strong field regions are present even at the end of the simulation.

A series of simulations with reduced-geometry targets finds that excluding Coulomb collisions leads to strong modification of the heat flux behavior that cannot match the experimental observation. In particular, in the foam case without collisions, no collimation or filamentation whatsoever is visible; there the hot electrons travel ballistically away from the acceleration region in a beam with an angular spread of over 90°. In the plasma case some heat flux filaments are seen, where they are caused by interface field and emerge from the nulls of that field as is seen in the collisional simulations presented above; the growth of that field region is independent of resistivity (absent the question of the origin of the convected field) so this result is to be expected.

VI. SUMMARY AND CONCLUSION

In summary, fast electron transport was shown experimentally to be dramatically different in multilayer foils with shock-rarefied plasma compared to the same unshocked CH foam or cold solid CH. The plasma layer resulted in reduced electron transport to the back of the target package by a factor of 25. Two-dimensional PIC modeling indicates that the transport is primarily affected by the self-generated magnetic fields, via two distinct but related phenomena. In both the rarefied plasma and initially cold foam Coulomb collisions lead to filamentation of the beam of hot electrons. In the foam the majority of the heat flux also collimates into a beam with a narrow spread, an effect not seen in the lower density plasma. In addition to this resistance-generated field, a strong insulating magnetic field is seen at the interface between the Au electron source and the plasma, caused by the convective flow of field with the return current. This field both directly impedes the electron flow into the CH region and affects the evolution of the heat flux filaments. These new findings shed light on fast electron behavior at material interfaces and contribute to the understanding of the underlying physics of electron transport in various media. These findings should be considered when designing multilayered targets for particle sources and will impact the fast ignition and shock ignition advanced inertial confinement fusion schemes in which electrons must transport across one or many sharp density interfaces.

ACKNOWLEGDMENTS

The authors are grateful to the OMEGA EP crew for the operations of four EP UV beams. The authors also acknowledge GA target design group for fruitful discussion. The work was supported by US Dept of Energy/NNSA under Contracts No. DE-FG52-09NA29033 (NLUF), No. DE-FC02-04ER54789 (FSC), No. DE-FG02-05ER54834 (ACE), and No. DE-NA0002953 and National Science Foundation under Grant No. ACI-1339893, and partially supported by the University of California Office of the President Lab Fee Grant No. LFR-17-449059. The simulations were performed on the Mira supercomputer at ALCF through the INCITE program.

[1] M. Tabak, J. Hammer, M. E. Glinsky, W. L. Kruer, S. C. Wilks, J. Woodworth, E. M. Campbell, and M. D. Perry, Phys. Plasmas **1**, 1626 (1994).

[2] S. Atzeni, Phys. Plasmas **6**, 3316 (1999).

[3] M. Honda, J. M. ter Vehn, and A. Pukhov, Phys. Plasmas **7**, 1302 (2000).

[4] Y. Sentoku, K. Mima, P. Kaw, and K. Nishikawa, Phys. Rev. Lett. **90**, 155001 (2003).

[5] R. G. Evans, Plasma Phys. Controlled Fusion **49**, B87 (2007).

[6] R. P. J. Town, C. Chen, L. A. Cottrill, M. H. Key, W. L. Kruer, A. B. Langdon, B. F. Lasinski, R. A. Snavely, C. H. Still, M. Tabak, D. R. Welch, and S. C. Wilks, Nucl. Instrum. Methods Phys. Res., Sect. A **544**, 61 (2005).

[7] M. S. Wei, A. A. Solodov, J. Pasley, R. B. Stephens, D. R. Welch, and F. N. Beg, Phys. Plasmas **15**, 083101 (2008).

[8] R. B. Stephens, R. A. Snavely, Y. Aglitskiy, F. Amiranoff, C. Andersen, D. Batani, S. D. Baton, T. Cowan, R. R. Freeman, T. Hall, S. P. Hatchett, J. M. Hill, M. H. Key, J. A. King, J. A. Koch, M. Koenig, A. J. MacKinnon, K. L. Lancaster, E. Martinolli, P. Norreys, E. Perelli-Cippo, M. Rabec Le Gloahec, C. Rousseaux, J. J. Santos, and F. Scianitti, Phys. Rev. E **69**, 066414 (2004).

[9] K. L. Lancaster, J. S. Green, D. S. Hey, K. U. Akli, J. R. Davies, R. J. Clarke, R. R. Freeman, H. Habara, M. H. Key, R. Kodama, K. Krushelnick, C. D. Murphy, M. Nakatsutsumi, P. Simpson, R. Stephens, C. Stoeckl, T. Yabuuchi, M. Zepf, and P. A. Norreys, Phys. Rev. Lett. **98**, 125002 (2007).

[10] F. Pérez, M. Koenig, D. Batani, S. D. Baton, F. N. Beg, C. Benedetti, E. Brambrink, S. Chawla, F. Dorchies, C. Fourment, M. Galimberti, L. A. Gizzi, R. Heathcote, D. P. Higginson, S. Hulin, R. Jafer, P. Koester, L. Labate, K. Lancaster, A. J. MacKinnon, A. G. McPhee, W. Nazarov, P. Nicolai, J. Pasley, A. Ravasio, M. Richetta, J. J. Santos, A. Sgattoni, C. Spindloe, B. Vauzour, and L. Volpe, Plasma Phys. Controlled Fusion **51**, 124035 (2009).

[11] B. Vauzour, F. Pérez, L. Volpe, K. Lancaster, P. Nicolaï, D. Batani, S. D. Baton, F. N. Beg, C. Benedetti, E. Brambrink, S. Chawla, F. Dorchies, C. Fourment, M. Galimberti, L. A. Gizzi, R. Heathcote, D. P. Higginson, S. Hulin, R. Jafer, P. Köster, L. Labate, A. J. MacKinnon, A. G. MacPhee, W. Nazarov, J. Pasley, C. Regan, X. Ribeyre, M. Richetta, G. Schurtz, A. Sgattoni, and J. J. Santos, Phys. Plasmas **18**, 043108 (2011).

[12] F. Pérez, A. Debayle, J. Honrubia, M. Koenig, D. Batani, S. D. Baton, F. N. Beg, C. Benedetti, E. Brambrink, S. Chawla, F. Dorchies, C. Fourment, M. Galimberti, L. A. Gizzi, L. Gremillet, R. Heathcote, D. P. Higginson, S. Hulin, R. Jafer, P. Koester, L. Labate, K. L. Lancaster, A. J. MacKinnon, A. G. MacPhee, W. Nazarov, P. Nicolai, J. Pasley, R. Ramis, M. Richetta, J. J. Santos, A. Sgattoni, C. Spindloe, B. Vauzour, T. Vinci, and L. Volpe, Phys. Rev. Lett. **107**, 065004 (2011).

[13] B. Vauzour, J. J. Santos, A. Debayle, S. Hulin, H.-P. Schlenvoigt, X. Vaisseau, D. Batani, S. D. Baton, J. J. Honrubia, P. Nicolaï, F. N. Beg, R. Benocci, S. Chawla, M. Coury, F. Dorchies, C. Fourment, E. d'Humières, L. C. Jarrot, P. McKenna, Y. J. Rhee, V. T. Tikhonchuk, L. Volpe, and V. Yahia, Phys. Rev. Lett. **109**, 255002 (2012).

[14] C. Stoeckl, J. A. Delettrez, J. H. Kelly, T. J. Kessler, B. E. Kruschwitz, S. J. Loucks, R. L. McCrory, D. D. Meyerhofer, D. N. Maywar, S. F. B. Morse, J. Myatt, A. L. Rigatti, L. J. Waxer, J. D. Zuegel, and R. B. Stephens, Fusion Sci. Technol. **49**, 367 (2006).

[15] H. Sawada, T. Yabuuchi, S. P. Regan, K. Anderson, M. S. Wei, R. Betti, J. Hund, M. H. Key, A. J. Mackinnon, H. S. McLean, R. R. Paguio, P. K. Patel, K. M. Saito, R. B. Stephens, S. C. Wilks, and F. N. Beg, High Energy Density Phys. **8**, 180 (2012).

[16] T. Yabuuchi, H. Sawada, S. P. Regan, K. Anderson, M. S. Wei, R. Betti, J. Hund, M. H. Key, A. J. Mackinnon, H. S. McLean, R. R. Paguio, P. K. Patel, K. M. Saito, R. B. Stephens, S. C. Wilks, and F. N. Beg, Phys. Plasmas **19**, 092705 (2012).

[17] C. Stoeckl, G. Fiksel, D. Guy, C. Mileham, P. M. Nilson, T. C. Sangster, M. J. Shoup III, and W. Theobald, Rev. Sci. Instrum. **83**, 033107 (2012).

[18] S. Chawla, M. S. Wei, R. Mishra, K. U. Akli, C. D. Chen, H. S. McLean, A. Morace, P. K. Patel, H. Sawada, Y. Sentoku, R. B. Stephens, and F. N. Beg, Phys. Rev. Lett. **110**, 025001 (2013).

[19] Y. Sentoku, E. d'Humières, L. Romagnani, P. Audebert, and J. Fuchs, Phys. Rev. Lett. **107**, 135005 (2011).

[20] R. A. Fonseca, L. O. Silva, F. S. Tsung, V. K. Decyk, W. Lu, C. Ren, W. B. Mori, S. Deng, S. Lee, T. Katsouleas, and J. C. Adam, Lect. Notes Comput. Sci. **2331**, 342 (2002).

[21] A. J. Kemp and L. Divol, Phys. Rev. Lett. **109**, 195005 (2012).

[22] J. May, J. Tonge, I. Ellis, W. B. Mori, F. Fiuza, R. A. Fonseca, L. O. Silva, and C. Ren, Phys. Plasmas **21**, 052703 (2014).

[23] F. Pérez, L. Gremillet, A. Decoster, M. Drouin, and E. Lefebvre, Phys. Plasmas **19**, 083104 (2012).

[24] N. A. Krall and A. W. Trivelpiece, *Principles of Plasma Physics* (McGraw-Hill, New York, 1973).

[25] A. R. Bell, J. R. Davies, and S. M. Guerin, Phys. Rev. E **58**, 2471 (1998).

[26] L. Gremillet, G. Bonnaud, and F. Amiranoff, Phys. Plasmas **9**, 941 (2002).

[27] J. May, J. Tonge, F. Fiuza, R. A. Fonseca, L. O. Silva, C. Ren, and W. B. Mori, Phys. Rev. E **84**, 025401 (2011).